

Generalized many-body exciton g-factors: magnetic hybridization and non-monotonic Rydberg series in monolayer WSe₂

Paulo E. Faria Junior,^{1,2,3,*} Daniel Hernangómez-Pérez,^{4,†}
Tomer Amit,^{5,‡} Jaroslav Fabian,³ and Sivan Refaely-Abramson⁵

¹*Department of Physics, University of Central Florida, Orlando, Florida 32816, USA*

²*Department of Electrical and Computer Engineering,
University of Central Florida, Orlando, Florida 32816, USA*

³*Institute of Theoretical Physics, University of Regensburg, 93040 Regensburg, Germany*

⁴*CIC nanoGUNE BRTA, Tolosa Hiribidea 76, 20018 San Sebastián, Spain*

⁵*Department of Molecular Chemistry and Materials Science,
Weizmann Institute of Science, Rehovot 7610001, Israel*

CONTENTS

I. Computational details	3
II. Operators representation in the excitonic basis	6
A. Preliminaries: basis set	6
B. Angular momentum operators in the excitonic basis	6
C. Generalized excitonic g-factor	8
III. Symmetry analysis	10
A. Zero magnetic field	10
B. Introducing the magnetic field	10
IV. Additional computational data	18
A. GW-BSE results of $S \in \{A_{\pm}, G, D\}$	18
V. Additional figures	20
References	23

* These authors contributed equally; corresponding author: paulo@ucf.edu

† These authors contributed equally; corresponding author: d.hernangomez@nanogune.eu

‡ These authors contributed equally.

I. COMPUTATIONAL DETAILS

Geometries. For our calculations, we considered the geometry of monolayer WSe₂ with an in-plane lattice parameter fixed to the experimental value of 3.289 Å [1, 2] with a Se-Se distance of 3.277 Å. A vacuum separation of 15.9 Å was considered in the out-of-plane direction to minimize interactions between periodic replicas.

Density functional theory

Quantum Espresso. We performed density functional theory (DFT) calculations using the QUANTUM ESPRESSO package [3–5]. For the exchange-correlation functional, we employed the non-empirical PBE generalized gradient approximation (GGA) [6]. QUANTUM ESPRESSO utilizes a plane-wave basis set, for which we set a kinetic energy cut-off of 90 Ry. Spin-orbit interaction was included by employing fully relativistic optimized norm-conserving Vanderbilt pseudopotentials from the PseudoDojo library [7]. The self-consistent charge density was converged on a $24 \times 24 \times 1$ **k**-point grid.

WIEN2k. To validate and cross-check DFT calculations performed within QUANTUM ESPRESSO, we also performed DFT calculations using the all-electron full-potential implementation of WIEN2k[8], one of the most accurate DFT codes available[9]. We also employed the PBE exchange-correlation functional, a **k**-grid of $30 \times 30 \times 1$, and a self-consistent convergence criteria of $10^{-6} e$ for the charge and 10^{-6} Ry for the energy. The core and valence electrons are separated by -6 Ry. We used orbital quantum numbers up to 10 within the atomic spheres and the plane-wave cutoff multiplied by the smallest radius of the muffin-tin sphere is set to 8. The radius of the muffin-tin sphere considered are 2.41 bohr for W and 2.30 bohr for S. For the inclusion of SOC, core electrons are considered fully relativistically and valence electrons are treated within a second variational step[10], with the scalar-relativistic wave functions calculated in an energy window from -10 to 8 Ry.

We find that the resulting DFT gap for the monolayer case at the K point is 1263.0 (1283.4) meV obtained with WIEN2k (QUANTUM ESPRESSO).

GW. We compute the quasi-particle energy spectrum within the GW approximation, using the BERKELEYGW package[11–14]. As a starting point, we use DFT energies and wavefunctions computed with QUANTUM ESPRESSO, then apply a one-shot non-self-consistent GW calculation (G_0W_0)[15], employed using the spinor implementation within

the `BERKELEYGW` package. This implementation includes non-perturbative spin-orbit coupling corrections[11, 14, 16]. The dielectric function was computed using the generalized plasmon-pole model of Hybertsen and Louie [15]. We used a $6 \times 6 \times 1$ uniform \mathbf{q} -grid, including a total of 4000 empty and occupied states, and applied a 25 Ry cut-off for the dielectric function. To accelerate convergence with respect to \mathbf{k} -point sampling, we refined the Brillouin zone sampling near $\mathbf{q} = \mathbf{0}$ by incorporating 10 additional \mathbf{q} -points within a non-uniform neck subsampling scheme [17]. The Coulomb interaction was truncated along the out-of-plane direction to prevent spurious coupling between periodic replicas [18]. We find a GW gap at the K point for the monolayer of 2311.63 meV, which is 1028.23 meV larger than the DFT gap.

BSE. The Bethe-Salpeter equation (BSE) was solved using the Tamm-Dancoff approximation (see also Sec. II A) within the `BERKELEYGW` package[11–14]. The electron-hole interaction kernel matrix elements of the Bethe-Salpeter Hamiltonian were computed on a uniform Monkhorst-Pack $24 \times 24 \times 1$ coarse \mathbf{k} -grid and subsequently interpolated to a $90 \times 90 \times 1$ uniform fine \mathbf{k} -grid, which was subsequently employed for the absorption and g-factor calculations. An energy cut-off of 5 Ry was applied to the dielectric matrix in the BSE electron-hole kernel matrix elements. The electron-hole kernel was computed including 24 bands (12 valence and 12 conduction). For the absorption calculations, a reduced set of 12 bands (6 valence and 6 conduction) was considered.

Orbital angular momentum matrix elements. Single-particle angular momentum matrix elements were calculated extending previous work by the some of the authors[19–21], see also Sec. II B. In the `QUANTUM ESPRESSO` calculations, we included a summation over 600 occupied and empty bands and checked the convergence of the results with respect to the total number of bands. For the calculation of the orbital angular momentum matrix elements, we used DFT energies and performed a scissor-shift of the conduction bands using the GW bandgap at the K point. In `WIEN2k` calculations, the energy window (-10 to 8 Ry) yields a total of 60 occupied and 1182 empty bands, enough to converge the orbital angular momentum calculations[21, 22].

Effective two-band model for excitons. The g-factors obtained within an effective two-band model follow the approach discussed in Refs. [22, 23] and do not incorporate off-diagonal terms neither in the single-particle nor in the exciton basis. Specifically, we treat conduction and valence bands with a parabolic dispersion with effective masses given by 0.2650 and -0.3519 , respectively, obtained from the WIEN2k calculations. The exciton wavefunctions are calculated considering the Rytova-Keldysh potential [24, 25] with an effective monolayer thickness of 6.55 \AA and a dielectric constant of 15.6 [26]. The dielectric constant of the surrounding dielectric environment is taken as $\varepsilon = 1$ to mimic air and $\varepsilon = 5$ to mimic hBN. The k -dependence of the X exciton g-factor has a convex dispersion with minimum at the K valley (consistent with previous calculations[22, 23, 27, 28]) and can be approximated by a parabola for $g_X(k) = g_X^{(0)} + g_X^{(2)}k^2$ with coefficients $g_X^{(0)} = -4.12$ and $g_X^{(2)} = 96.84$ (these values include the scissor shift in the band gap, see also Table I). Within this approach, the exciton g-factor, i.e., the single-particle parabolic dependence $g_X(k)$ weighted by the exciton wavefunction $F(k)$ from the two-band model (see also Eq. S12), we found $g_X = 2\pi \int dk k g_X(k) |F(k)|^2 = g_X^{(0)} + 2\pi g_X^{(2)} \int dk k^3 |F(k)|^2$. The numerical grid used for the exciton energies and wavefunctions considers a circular region with radius 0.5 \AA extracted from a 181×181 square grid from -0.5 \AA to 0.5 \AA , leading to 25445 effective k-points. The binding energies for the 1s, 2s, 3s, and 4s states are 430.2 (131.2) meV, 186.5 (25.7) meV, 109.5 (10.2) meV, and 71.8 (5.8) meV, respectively, for $\varepsilon = 1$ ($\varepsilon = 5$).

II. OPERATORS REPRESENTATION IN THE EXCITONIC BASIS

A. Preliminaries: basis set

In this work, we consider the ensemble of excitons $\{|S\rangle\}$ with energies $\{\Omega_S\}$, which are obtained by numerically solving the BSE within the Tamm-Dancoff approximation[13] for a finite number of conduction and valence quasi-particle bands. This equation is an effective eigenvalue problem $\hat{H}^{\text{BSE}}|S\rangle = \Omega_S|S\rangle$, where the matrix elements of the Hamiltonian written in the electron-hole basis read

$$\hat{H}_{c\mathbf{k};c'v'\mathbf{k}'}^{\text{BSE}} = (E_{c\mathbf{k}} - E_{v\mathbf{k}})\delta_{c,c'}\delta_{v,v'}\delta_{\mathbf{k},\mathbf{k}'} + K_{v\mathbf{k};v'c'\mathbf{k}'}^{\text{eh}}. \quad (\text{S1})$$

Here, $E_{c\mathbf{k}}$ (resp. $E_{v\mathbf{k}}$) are the quasi-particle energies of the conduction (resp. valence) bands, $K_{v\mathbf{k};v'c'\mathbf{k}'}^{\text{eh}} = \langle v\mathbf{k}|\hat{K}^{\text{eh}}|v'c'\mathbf{k}'\rangle$ are the matrix elements of the electron-hole interaction kernel.

It is understood that by employing this equation, each exciton state is expressed as the coherent superposition of electron-hole pairs

$$|S\rangle = \sum_{v\mathbf{k}} \mathcal{A}_{v\mathbf{k}}^S |v\mathbf{k}\rangle |c\mathbf{k}\rangle, \quad (\text{S2})$$

where $\mathcal{A}_{v\mathbf{k}}^S$ is the exciton amplitude and $|v\mathbf{k}\rangle |c\mathbf{k}\rangle$ is a short-hand notation for $|v\mathbf{k}\rangle \otimes |c\mathbf{k}\rangle$. In other words, exciton states are spanned in the conduction-valence (or electron-hole) basis, which belongs to the tensor product space $\mathcal{H}_{\text{ex}} = \mathcal{H}_e \otimes \mathcal{H}_h$. For simplicity in this work, we only consider the case of direct excitons, assuming negligible coupling to phonons or electrons and a vanishingly small momentum transfer coming from the absorbed light.

B. Angular momentum operators in the excitonic basis

We start our derivations by considering the exciton spin operators. The exciton spin operator directed along the spatial direction $\hat{\epsilon}$, with $\epsilon = x, y, z$, is defined as

$$\hat{\Sigma}^\epsilon = \hat{\Sigma}_e^\epsilon + \hat{\Sigma}_h^\epsilon := \hat{\Sigma}_e^\epsilon \otimes \mathbb{1}_h - \mathbb{1}_e \otimes \hat{\Sigma}_h^\epsilon, \quad (\text{S3})$$

where the minus sign is related to the definition of the hole operator and we promoted the single-particle operators in the electron and hole subspaces to combined electron-hole Hilbert space by using a tensor product with the 2×2 identity operator, $\mathbb{1}$, in each respective subspace. Each spin operator is a matrix, with its elements given in the Bloch basis, $|\alpha\mathbf{k}\rangle$, by

$$\Sigma_{\alpha\alpha'\mathbf{k}}^\epsilon = \langle \alpha\mathbf{k} | \sigma^\epsilon | \alpha'\mathbf{k} \rangle, \quad (\text{S4})$$

and measured in units of $\hbar/2$. Here, σ^ϵ correspond to the Pauli matrices, with the following representation

$$\sigma^x = \begin{pmatrix} 0 & 1 \\ 1 & 0 \end{pmatrix}, \quad \sigma^y = \begin{pmatrix} 0 & -i \\ i & 0 \end{pmatrix}, \quad \sigma^z = \begin{pmatrix} 1 & 0 \\ 0 & -1 \end{pmatrix}. \quad (\text{S5})$$

Using Eq. S3, we can explicitly compute matrix elements of the operator in the excitonic basis to find

$$\langle S | \hat{\Sigma}^\epsilon | S' \rangle = \sum_{v\mathbf{k}} \left[\sum_{c'} (\mathcal{A}_{v\mathbf{c}\mathbf{k}}^S)^* \mathcal{A}_{v'c'\mathbf{k}}^{S'} \Sigma_{cc'\mathbf{k}}^\epsilon - \sum_{v'} (\mathcal{A}_{v\mathbf{c}\mathbf{k}}^S)^* \mathcal{A}_{v'c\mathbf{k}}^{S'} \Sigma_{vv'\mathbf{k}}^\epsilon \right]. \quad (\text{S6})$$

In the absence of degenerate excitonic subspaces, only the diagonal components of Eq. (S6), $\langle \hat{\Sigma}^\epsilon \rangle_S := \langle S | \hat{\Sigma}^\epsilon | S \rangle$ would be necessary, thus, Eq. (S6) simplifies to

$$\langle \hat{\Sigma}^\epsilon \rangle_S = \sum_{v\mathbf{k}} \left[\sum_{c'} (\mathcal{A}_{v\mathbf{c}\mathbf{k}}^S)^* \mathcal{A}_{vc'\mathbf{k}}^S \Sigma_{cc'\mathbf{k}}^\epsilon - \sum_{v'} (\mathcal{A}_{v\mathbf{c}\mathbf{k}}^S)^* \mathcal{A}_{v'c\mathbf{k}}^S \Sigma_{vv'\mathbf{k}}^\epsilon \right], \quad (\text{S7})$$

Furthermore, if the spin is a good quantum number at the single-particle level, so that all the transitions are also spin-conserving and the single-particle spin operator is diagonal in the Bloch basis, we find the simplified form

$$\langle \hat{\Sigma}^\epsilon \rangle_S = \sum_{v\mathbf{k}} |\mathcal{A}_{v\mathbf{c}\mathbf{k}}^S|^2 (\Sigma_{c\mathbf{k}}^\epsilon - \Sigma_{v\mathbf{k}}^\epsilon), \quad (\text{S8})$$

where $\Sigma_{\alpha\mathbf{k}}^\epsilon := \Sigma_{\alpha\alpha\mathbf{k}}^\epsilon$. This expression was already suggested in Ref. 29 when considering the expectation value of the spin of non-degenerate excitons in the $\hat{\mathbf{z}}$ direction in Bi/SiC. We also note that similar approaches to the one described here have recently been used to investigate exciton effects on the shift current. [30]

The orbital angular momentum can be decomposed in an analogous way to Eq. (S3). For the single-particle states, we follow Ref. 19, and the matrix elements in the Bloch basis of the (symmetrized) angular momentum operator (here we choose for simplicity the $\hat{\mathbf{z}}$ direction, but the matrix elements in the $\hat{\mathbf{x}}$ and $\hat{\mathbf{y}}$ directions are obtained by a straightforward permutation of indices) can be written as

$$L_{\alpha\alpha'\mathbf{k}}^z = \frac{1}{im_0} \left[\sum'_{\beta \neq \alpha} \frac{p_{\alpha\beta\mathbf{k}}^x p_{\beta\alpha'\mathbf{k}}^y - p_{\alpha\beta\mathbf{k}}^y p_{\beta\alpha'\mathbf{k}}^x}{\epsilon_{\alpha\mathbf{k}} - \epsilon_{\beta\mathbf{k}}} - \sum'_{\beta \neq \alpha'} \frac{p_{\alpha\beta\mathbf{k}}^y p_{\beta\alpha'\mathbf{k}}^x - p_{\alpha\beta\mathbf{k}}^x p_{\beta\alpha'\mathbf{k}}^y}{\epsilon_{\alpha'\mathbf{k}} - \epsilon_{\beta\mathbf{k}}} \right], \quad (\text{S9})$$

where we employed units of $\mathcal{B}_z = \mu_B B_z$. Here, the Bohr's magneton is given by $\mu_B = |e|\hbar/(2m_0)$, B_z is the external applied magnetic field along $\hat{\mathbf{z}}$, $p_{\alpha\beta\mathbf{k}}^\epsilon$ corresponds to the matrix elements of the canonical momentum in the Bloch basis and $\epsilon_{\alpha\mathbf{k}}$ are the Kohn-Sham (or GW) energies. The \prime symbol in the first (second) summation indicates that the α' (α) state must be excluded if α and α' are in the same degenerate subset, leading to the equation

$$L_{\alpha\alpha'\mathbf{k}}^z = \frac{1}{im_0} \sum_{\beta \neq \alpha, \alpha'} \left[\frac{p_{\alpha\beta\mathbf{k}}^x p_{\beta\alpha'\mathbf{k}}^y - p_{\alpha\beta\mathbf{k}}^y p_{\beta\alpha'\mathbf{k}}^x}{\epsilon_{\alpha\mathbf{k}} - \epsilon_{\beta\mathbf{k}}} - \frac{p_{\alpha\beta\mathbf{k}}^y p_{\beta\alpha'\mathbf{k}}^x - p_{\alpha\beta\mathbf{k}}^x p_{\beta\alpha'\mathbf{k}}^y}{\epsilon_{\alpha'\mathbf{k}} - \epsilon_{\beta\mathbf{k}}} \right]. \quad (\text{S10})$$

We note that expressions (S9) and (S10) naturally take into account degenerate single-particle states and can be derived within the context of the $\mathbf{k}\cdot\mathbf{p}$ perturbation theory or by employing the relation between the position operator and the Berry connection [31–33].

Following the same steps as for the exciton spin, the excitonic matrix elements of the angular momentum operator in the $\hat{\mathbf{e}}$ direction simply read

$$\langle S | \hat{L}^\epsilon | S' \rangle = \sum_{v\mathbf{k}} \left[\sum_{c'} (\mathcal{A}_{v\mathbf{k}}^S)^* \mathcal{A}_{vc'\mathbf{k}}^{S'} L_{cc'\mathbf{k}}^\epsilon - \sum_{v'} (\mathcal{A}_{v\mathbf{k}}^S)^* \mathcal{A}_{v'\mathbf{k}}^{S'} L_{v'v\mathbf{k}}^\epsilon \right],$$

with $L_{\alpha\alpha'\mathbf{k}}^\epsilon = \langle \alpha\mathbf{k} | \hat{L}^\epsilon | \alpha'\mathbf{k} \rangle$.

C. Generalized excitonic g-factor

We now define the operator $\hat{\mathbf{g}} := \hat{\mathbf{L}} + \hat{\mathbf{\Sigma}}$, where we considered $g_0 \simeq 2$, so that each component of this vector operator is expressed in reduced units of $\mathcal{B}_\epsilon := \mu_B B_\epsilon$. Straightforwardly inherited from its angular momentum composition, and as shown in Sec. II B, the exciton

g-factor is in general not diagonal in the excitonic basis. We can easily obtain the general matrix elements once the angular momentum matrix elements are known,

$$\langle S|\hat{g}^\epsilon|S'\rangle = \sum_{v\mathbf{k}} \left[\sum_{c'} (\mathcal{A}_{v\mathbf{c}\mathbf{k}}^S)^* \mathcal{A}_{vc'\mathbf{k}}^{S'} g_{cc'\mathbf{k}}^\epsilon - \sum_{v'} (\mathcal{A}_{v\mathbf{c}\mathbf{k}}^S)^* \mathcal{A}_{v'\mathbf{c}\mathbf{k}}^{S'} g_{vv'\mathbf{k}}^\epsilon \right], \quad (\text{S11})$$

with $g_{\alpha\alpha'\mathbf{k}}^\epsilon = L_{\alpha\alpha'\mathbf{k}}^\epsilon + \Sigma_{\alpha\alpha'\mathbf{k}}^\epsilon$.

Importantly, this expression for the exciton g-factor generalizes the one employed in previous works[20, 27], where degenerate exciton subspaces were not taken into consideration and thus only the diagonal matrix elements, as well as only the out-of-plane $\hat{\mathbf{z}}$ direction, $\langle \hat{g}^z \rangle_S := \langle S|\hat{g}^z|S\rangle$, was considered,

$$\langle \hat{g}^z \rangle_S = \sum_{v\mathbf{k}} |\mathcal{A}_{v\mathbf{c}\mathbf{k}}^S|^2 (g_{c\mathbf{k}}^z - g_{v\mathbf{k}}^z), \quad (\text{S12})$$

where $g_{\alpha\mathbf{k}}^z = L_{\alpha\mathbf{k}}^z + \Sigma_{\alpha\mathbf{k}}^z$.

III. SYMMETRY ANALYSIS

The group theory nomenclature used here follows Ref. 34.

A. Zero magnetic field

The dipole matrix element mediated by the linear momentum operator between conduction (c) and valence (v) bands is given as $\mathbf{p}_{cv}^\epsilon = \langle c, \pm\mathbf{K} | \mathbf{p} \cdot \hat{\epsilon} | v, \pm\mathbf{K} \rangle$. Within group theory $\mathbf{p}_{cv}^\epsilon = \Gamma_c^* \otimes \Gamma_\epsilon \otimes \Gamma_v$, with $\Gamma_{c(v)}$ being the irreps of conduction (valence) bands and Γ_ϵ is the irrep of the vector coordinate $\epsilon = x, y, z$. The transition $\text{CB}_- \rightarrow \text{VB}_+$ at \mathbf{K} ($-\mathbf{K}$) yields $K_8^* \otimes K_{10} = K_4$ ($K_7^* \otimes K_9 = K_4$), while $\text{CB}_+ \rightarrow \text{VB}_+$ at \mathbf{K} ($-\mathbf{K}$) yields $K_7^* \otimes K_{10} = K_3$ ($K_8^* \otimes K_9 = K_2$). The irreps related to the in-plane circular polarization (s_\pm) are $K_2 \sim x - iy$, $K_3 \sim x + iy$ and for out-of-plane linear polarization (z), the irrep is $K_4 \sim z$.

B. Introducing the magnetic field

In transition metal dichalcogenide (TMDC) monolayers, the low energy excitons with zero-momentum (located at the Γ point) have the following irreducible representations (irreps) within the D_{3h} symmetry group:

$$\begin{aligned} \text{Bright}(A) &\sim \Gamma_6 \sim \{x, y\} \rightarrow 2 \text{ dimensional,} \\ \text{Grey}(G) &\sim \Gamma_4 \sim z \rightarrow 1 \text{ dimensional,} \\ \text{Dark}(D) &\sim \Gamma_3 \rightarrow 1 \text{ dimensional.} \end{aligned} \tag{S13}$$

Based on symmetry considerations, we can derive the Hamiltonian for the Zeeman splitting for these low energy states. Specifically, the Hamiltonian term that couples to the magnetic field reads:

$$\hat{H}_Z(\mathbf{B}) = \hat{H}_x \hat{\mathbf{x}} + \hat{H}_y \hat{\mathbf{y}} + \hat{H}_z \hat{\mathbf{z}}, \tag{S14}$$

with

$$\hat{H}_\epsilon := \hat{g}^\epsilon \mu_B B_\epsilon = \hat{g}^\epsilon \mathcal{B}_\epsilon, \tag{S15}$$

and where we remind that $\mathcal{B}_\epsilon := \mu_B B_\epsilon$, with $\epsilon = x, y, z$ and μ_B is the Bohr magneton.

The components of the magnetic field Hamiltonian transform as pseudo-vectors, *i.e.*:

$$\begin{aligned}\{H_x, H_y\} &\sim \{R_x, R_y\} \sim \Gamma_5 \\ H_z &\sim R_z \sim \Gamma_2.\end{aligned}\tag{S16}$$

By performing the direct product between the irreps of the excitons, we can immediately reveal how the external magnetic field will couple the different exciton states. We find

$$\begin{aligned}A - A &: \Gamma_6 \otimes \Gamma_6 = \Gamma_1 \oplus \Gamma_2 \oplus \Gamma_6, \\ A - G &: \Gamma_6 \otimes \Gamma_4 = \Gamma_5, \\ A - D &: \Gamma_6 \otimes \Gamma_3 = \Gamma_5, \\ G - D &: \Gamma_4 \otimes \Gamma_3 = \Gamma_2,\end{aligned}\tag{S17}$$

which indicates that the A exciton subspace couples with $\mathbf{B} \parallel \hat{\mathbf{z}}$, that G and D excitons couple with $\mathbf{B} \parallel \hat{\mathbf{z}}$, and that the A exciton couples with G and D excitons via $\mathbf{B} \perp \hat{\mathbf{z}}$.

Using this information, the Hamiltonian in Eq. (S14) reads in matrix form

$$H_Z(\mathbf{B}) = \begin{bmatrix} g_A \mathcal{B}_z \otimes M_A & g_{AG} \mathcal{B}_{xy} \otimes M_{AG} & g_{AD} \mathcal{B}_{xy} \otimes M_{AD} \\ & 0 & g_{GD} \mathcal{B}_z \otimes M_{GD} \\ \text{c.c.} & & 0 \end{bmatrix},\tag{S18}$$

where g_A is the A -exciton g -factor, g_{GD} is the g -factor coupling G and D excitons, g_{AG} and g_{AD} are g -factors that coupling A - G and A - D excitons, respectively. The matrices M_A (2×2), M_{AG} (2×1), M_{AD} (2×1), and M_{GD} (1×1) incorporate complex values related to the particular choice of the exciton basis. We emphasize that the most crucial information given by the symmetry-based Hamiltonian is that $\mathbf{B} \parallel \hat{\mathbf{z}}$ cannot mix A and G, D excitons. This can only be achieved with in-plane ($\mathbf{B} \perp \hat{\mathbf{z}}$) fields.

Let us further elaborate on the choice of the basis set to the Hamiltonian S18. The

symmetry relations for pseudovector operators acting on the states of Eq. S13 are given by

$$\begin{aligned}
\langle \Gamma_6^1 | w_z | \Gamma_6^2 \rangle &= -\langle \Gamma_6^2 | w_z | \Gamma_6^1 \rangle, \\
\langle \Gamma_6^1 | w_x | \Gamma_3 \rangle &= \langle \Gamma_6^2 | w_y | \Gamma_3 \rangle, \\
\langle \Gamma_6^2 | w_x | \Gamma_4 \rangle &= -\langle \Gamma_6^1 | w_y | \Gamma_4 \rangle.
\end{aligned} \tag{S19}$$

By choosing the basis set as $\{|\Gamma_6^+\rangle, |\Gamma_6^-\rangle, |\Gamma_4\rangle, |\Gamma_3\rangle\}$ (Γ_6^\pm relates to fully circularly polarization, s_\pm), the Hamiltonian takes the form

$$H_Z(\mathbf{B}) = \begin{bmatrix} +g_A \mathcal{B}_z & 0 & i\alpha_{AG} g_{AG} \mathcal{B}_- & \alpha_{AD} g_{AD} \mathcal{B}_- \\ 0 & -g_A \mathcal{B}_z & -i\alpha_{AG} g_{AG} \mathcal{B}_+ & \alpha_{AD} g_{AD} \mathcal{B}_+ \\ & & 0 & \alpha_{GD} g_{GD} \mathcal{B}_z \\ \text{c.c} & & \alpha_{GD}^* g_{GD} \mathcal{B}_z & 0 \end{bmatrix}, \tag{S20}$$

with $\mathcal{B}_\pm = (\mathcal{B}_x \pm i\mathcal{B}_y) / \sqrt{2}$. Note how the coefficients depend on the choice of basis. In the numerical calculations within the GW-BSE formalism, we do not expect the Hamiltonian to take such a intuitive form since the exciton basis will very likely a superposition of this well-defined basis. Such “mixed” basis are not only restricted to GW-BSE calculations. They are, in fact, a common outcome from first principles calculations whenever the bands (or irreps) are degenerate (or nearly degenerate)[35–38].

At this point, the non-zero matrix elements allowed by symmetry (Eqs. S18 and S20) provide the right functional form for the magnetic field dependence, which is particularly relevant for fitting experimental data. However, the g-factor terms do not have a precise meaning without a proper connection to the relevant energies and states that constitute each exciton. In order to do so and provide a microscopic foundation for the symmetry-based Hamiltonian, we can approximate the exciton states by the coefficient directly at the K

valleys, as previously considered in other works[39–41]

$$\begin{aligned}
|A_+\rangle &= |\text{VB}_+, K\rangle |\text{CB}_+, K\rangle, \\
|A_-\rangle &= |\text{VB}_+, -K\rangle |\text{CB}_+, -K\rangle, \\
|G\rangle &= \frac{1}{\sqrt{2}} (|\text{VB}_+, K\rangle |\text{CB}_-, K\rangle + |\text{VB}_+, -K\rangle |\text{CB}_-, -K\rangle), \\
|D\rangle &= \frac{1}{\sqrt{2}} (|\text{VB}_+, K\rangle |\text{CB}_-, K\rangle - |\text{VB}_+, -K\rangle |\text{CB}_-, -K\rangle).
\end{aligned} \tag{S21}$$

To verify that this approximation to the full exciton states satisfies the symmetry considerations of Eq. (S13), we can evaluate the optical selection rules given by the matrix elements

$$\langle \emptyset | \mathbf{p} | S \rangle = \sum_{v\mathbf{k}} \mathcal{A}_{v\mathbf{k}}^S \langle c\mathbf{k} | \mathbf{p} | v\mathbf{k} \rangle, \tag{S22}$$

where, $|\emptyset\rangle$ corresponds to the ground state (Fermi sea), $S \in \{A_\pm, G, D\}$ and $\mathcal{A}_{v\mathbf{k}}^S$ is the exciton amplitude of the S -th exciton, solution of the BSE, see Eq. (S2).

The single-particle selection rules are given by

$$\left\langle \text{CB}_+, \pm K \left| \mathbf{p} \cdot \frac{(\hat{x} \pm i\hat{y})}{\sqrt{2}} \right| \text{VB}_+, \pm K \right\rangle = \gamma \left(\frac{1 \pm i}{\sqrt{2}} \right), \tag{S23}$$

$$\langle \text{CB}_-, +K | \mathbf{p} \cdot \hat{z} | \text{VB}_+, +K \rangle = |\langle \text{CB}_-, -K | \mathbf{p} \cdot \hat{z} | \text{VB}_+, -K \rangle| = \gamma_z,$$

thus, it follows that the exciton selection rules are given by

$$\begin{aligned}
|\langle A_\pm | \mathbf{p} \cdot \hat{\alpha} | 0 \rangle|^2 &= \left| \left\langle \text{CB}_+, \pm K \left| \mathbf{p} \cdot \left(\frac{\hat{x} \pm i\hat{y}}{\sqrt{2}} \right) \right| \text{VB}_+, \pm K \right\rangle \right|^2, \\
&= \gamma^2.
\end{aligned} \tag{S24}$$

$$\begin{aligned}
|\langle G | \mathbf{p} \cdot \hat{\alpha} | 0 \rangle|^2 &= \frac{1}{2} |\langle \text{CB}_-, K | \mathbf{p} \cdot \hat{z} | \text{VB}_+, K \rangle + \langle \text{CB}_-, -K | \mathbf{p} \cdot \hat{z} | \text{VB}_+, -K \rangle|^2, \\
&= \frac{1}{2} |\gamma_z + \gamma_z|^2, \\
&= 2\gamma_z^2.
\end{aligned} \tag{S25}$$

$$\begin{aligned}
|\langle D | \mathbf{p} \cdot \hat{\alpha} | 0 \rangle|^2 &= \frac{1}{2} |\langle \text{CB}_-, K | \mathbf{p} \cdot \hat{z} | \text{VB}_+, K \rangle - \langle \text{CB}_-, -K | \mathbf{p} \cdot \hat{z} | \text{VB}_+, -K \rangle|^2, \\
&= \frac{1}{2} |\gamma_z - \gamma_z|^2, \\
&= 0,
\end{aligned} \tag{S26}$$

with γ and γ_z differing by 2 orders of magnitude ($\gamma \gg \gamma_z$). It is important to emphasize here that γ_z is rather small because of the small overlap between the wavefunctions with nearly opposite spin, i. e., VB_+ (nearly totally spin-up at K) and CB_- (nearly totally spin-down at K)[21].

Besides evaluating the dipole matrix elements for these excitonic transitions, we also verify that this basis set satisfy the irreps of Eq. S13 with respect to the mirror plane symmetry operation, $\hat{\sigma}_v$ (crossing the M points of the first Brillouin zone, as shown in Fig. 1 of the main text). By inspecting the character table of the D_{3h} group for the mirror plane(s) symmetry operation, we extract a character of 0 for the A excitons, 1 for the G exciton, -1 for the D exciton. The effect of $\hat{\sigma}_v$ on the exciton basis can be written as

$$\hat{\sigma}_v A_+ = A_-, \tag{S27}$$

$$\hat{\sigma}_v A_- = A_+, \tag{S28}$$

$$\hat{\sigma}_v G = G, \tag{S29}$$

$$\hat{\sigma}_v D = -D, \tag{S30}$$

in which the sign for the D exciton is directly connected to the sign change between K and $-K$ points, as given in Eq. S21, consequence of intervalley exchange coupling [41].

Let us now evaluate the exciton spin matrix elements for magnetic fields along z and along x directions using Eqs. (S4) and (S6). For the subset $|\text{CB}_+, \pm K\rangle, |\text{CB}_-, \pm K\rangle, |\text{VB}_+, \pm K\rangle$, numerical evaluations within DFT give

$$\Sigma_K^z = \begin{bmatrix} \sigma_{\text{CB}_+} & 0 & 0 \\ 0 & \sigma_{\text{CB}_-} & 0 \\ 0 & 0 & \sigma_{\text{VB}_+} \end{bmatrix}, \quad \Sigma_K^x = \begin{bmatrix} 0 & \sigma_{\text{CB}} & 0 \\ \sigma_{\text{CB}} & 0 & 0 \\ 0 & 0 & 0 \end{bmatrix}, \quad \Sigma_{-K}^e = -\Sigma_K^e \tag{S31}$$

with the explicit matrix elements expressed as

$$\begin{aligned}
\sigma_{\text{CB}_+} &= \langle \text{CB}_+ | \sigma_z | \text{CB}_+ \rangle, \\
\sigma_{\text{CB}_-} &= \langle \text{CB}_- | \sigma_z | \text{CB}_- \rangle, \\
\sigma_{\text{VB}_+} &= \langle \text{VB}_+ | \sigma_z | \text{VB}_+ \rangle, \\
\sigma_{\text{CB}} &= \langle \text{CB}_+ | \sigma_{x(y)} | \text{CB}_- \rangle.
\end{aligned} \tag{S32}$$

The values obtained using QUANTUM ESPRESSO and Wien2k are given in Table I.

In this basis, the exciton spin matrix elements in the $\epsilon = z$ direction are

$$\begin{aligned}
\langle S | \hat{\Sigma}^z | S' \rangle &= \left[(\mathcal{A}_{\text{VB}_+, \text{CB}_+, +K}^S)^* \mathcal{A}_{\text{VB}_+, \text{CB}_+, +K}^{S'} - (\mathcal{A}_{\text{VB}_+, \text{CB}_+, -K}^S)^* \mathcal{A}_{\text{VB}_+, \text{CB}_+, -K}^{S'} \right] [\sigma_{\text{CB}_+} - \sigma_{\text{VB}_+}] \\
&+ \left[(\mathcal{A}_{\text{VB}_+, \text{CB}_-, +K}^S)^* \mathcal{A}_{\text{VB}_+, \text{CB}_-, +K}^{S'} - (\mathcal{A}_{\text{VB}_+, \text{CB}_-, -K}^S)^* \mathcal{A}_{\text{VB}_+, \text{CB}_-, -K}^{S'} \right] [\sigma_{\text{CB}_-} - \sigma_{\text{VB}_+}],
\end{aligned} \tag{S33}$$

$$\begin{aligned}
S = S' \Rightarrow \langle S | \hat{\Sigma}^\epsilon | S \rangle &= \left[|\mathcal{A}_{\text{VB}_+, \text{CB}_+, +K}^S|^2 - |\mathcal{A}_{\text{VB}_+, \text{CB}_+, -K}^S|^2 \right] [\sigma_{\text{CB}_+} - \sigma_{\text{VB}_+}] \\
&+ \left[|\mathcal{A}_{\text{VB}_+, \text{CB}_-, +K}^S|^2 - |\mathcal{A}_{\text{VB}_+, \text{CB}_-, -K}^S|^2 \right] [\sigma_{\text{CB}_-} - \sigma_{\text{VB}_+}],
\end{aligned} \tag{S34}$$

$$\hat{\Sigma}^z = \left[\begin{array}{cc|cc} +\sigma_{\text{CB}_+} - \sigma_{\text{VB}_+} & 0 & 0 & 0 \\ 0 & -\sigma_{\text{CB}_+} + \sigma_{\text{VB}_+} & 0 & 0 \\ \hline 0 & 0 & 0 & \sigma_{\text{CB}_-} - \sigma_{\text{VB}_+} \\ 0 & 0 & \sigma_{\text{CB}_-} - \sigma_{\text{VB}_+} & 0 \end{array} \right]. \tag{S35}$$

The exciton spin matrix elements for $\epsilon = x$ are

$$\begin{aligned}
\langle S | \hat{\Sigma}^x | S' \rangle &= \left[(\mathcal{A}_{\text{CB}_+, \text{VB}_+, +K}^S)^* \mathcal{A}_{\text{CB}_-, \text{VB}_+, +K}^{S'} - (\mathcal{A}_{\text{CB}_+, \text{VB}_+, -K}^S)^* \mathcal{A}_{\text{CB}_-, \text{VB}_+, -K}^{S'} \right] \sigma_{\text{CB}} \\
&+ \left[(\mathcal{A}_{\text{CB}_-, \text{CB}_+, +K}^S)^* \mathcal{A}_{\text{CB}_+, \text{VB}_+, +K}^{S'} - (\mathcal{A}_{\text{CB}_-, \text{VB}_+, -K}^S)^* \mathcal{A}_{\text{CB}_+, \text{CB}_+, -K}^{S'} \right] \sigma_{\text{CB}},
\end{aligned} \tag{S36}$$

$$\hat{\Sigma}^x = \frac{\sigma_{CB}}{\sqrt{2}} \left[\begin{array}{cc|cc} 0 & 0 & 1 & 1 \\ 0 & 0 & -1 & 1 \\ \hline 1 & -1 & 0 & 0 \\ 1 & 1 & 0 & 0 \end{array} \right]. \quad (\text{S37})$$

We finally obtain the total Hamiltonian, $\hat{H} = \hat{H}^{\text{BSE}} + \hat{\mathbf{g}} \cdot \mathbf{B}$, including the zero field diagonal part and a Zeeman term for a magnetic field along the the xz plane

$$H = \left[\begin{array}{cc|cc} \Delta + g_A \mathcal{B} \cos \theta & 0 & g_{AG} \mathcal{B} \sin \theta & g_{AD} \mathcal{B} \sin \theta \\ 0 & \Delta - g_A \mathcal{B} \cos \theta & -g_{AG} \mathcal{B} \sin \theta & g_{AD} \mathcal{B} \sin \theta \\ \hline g_{AG} \mathcal{B} \sin \theta & -g_{AG} \mathcal{B} \sin \theta & \delta & g_{GD} \mathcal{B} \cos \theta \\ g_{AD} \mathcal{B} \sin \theta & g_{AD} \mathcal{B} \sin \theta & g_{GD} \mathcal{B} \cos \theta & 0 \end{array} \right]. \quad (\text{S38})$$

with $\mathcal{B} = \mu_B B$. We have two limiting cases, $\theta = 0 \Rightarrow \mathbf{B} = B\hat{\mathbf{z}}$ and $\theta = 90^\circ \Rightarrow \mathbf{B} = B\hat{\mathbf{x}}$. The exciton energy splittings can be fitted to our GW-BSE results, $\Delta = 54.8$ meV and $\delta = 2.4$ meV, and the g-factor values can be numerically calculated directly at the K-point, $g_A = g_{CB_+} - g_{VB_+} = -2.1$, $g_{GD} = g_{CB_-} - g_{VB_+} = -4.371$, $g_{AG} = g_{AD} = g_{CB}/\sqrt{2} = 0.847$. The (single-particle) band g-factors are obtained from the QUANTUM ESPRESSO calculations with a GW scissor shift operation[20], and they are given in Table I. In the same table, we also compare the QUANTUM ESPRESSO calculated values with WIEN2k to verify that both DFT codes give very similar results.

Table I. Numerical values for spin and orbital angular momenta. In parentheses, DFT indicates that the operator was calculated using DFT energies, GW refers to a rigid scissor shift correction using the GW band gap obtained at the K point, and SC denotes a rigid scissor shift of 1 eV. While the values of σ and L in the z -direction are real within the calculations, they are complex for the x, y directions due to the presence of (arbitrary) complex phases. However, for our purposes here, it suffices to consider the absolute value.

		VB ₊	CB ₋	CB ₊	CB(xy)
QUANTUM	σ	0.999	-0.917	0.977	0.973
ESPRESSO	L (DFT)	5.348	2.040	3.134	0.209
	g (DFT)	6.347	1.123	4.111	1.182
	L (GW)	3.754	1.199	1.676	0.225
	g (GW)	4.753	0.282	2.653	1.198
WIEN2k	σ	0.999	-0.921	0.977	0.974
	L (DFT)	5.310	1.962	3.140	0.064
	g (DFT)	6.310	1.042	4.117	1.038
	L (SC)	3.716	1.155	1.676	0.088
	g (SC)	4.716	0.234	2.656	1.062

IV. ADDITIONAL COMPUTATIONAL DATA

A. GW-BSE results of $S \in \{A_{\pm}, G, D\}$

Table II we summarize the energies and oscillator strengths calculated with the GW-BSE formalism.

Table II. Excitonic energies and oscillator strengths for the low-energy $\{S\} = \{A_{\pm}, G, D\}$ in monolayer WSe₂. Energy values are given in meV and oscillator strengths in units of $e^2 a_0^2$. The (bright-grey) A-G splitting is 52.4 meV while the (grey-dark) G-D splitting is 2.4 meV. This subspace is well-separated of the other excitons, as the next exciton state is ~ 164 meV above the A exciton.

Exciton	Energy	$ P_+ ^2$	$ P_- ^2$	$ P_z ^2$	Irrep
A	1771.58	783.025	4771.892	–	Γ_6
	1771.52	4775.531	786.309	–	
G	1719.14	–	–	9.562	Γ_4
D	1716.77	–	–	0.001	Γ_3

The numerical values of the spin matrices obtained via Eq. S6 and the orbital angular momentum matrices obtained via Eq. S11 in the basis of $S \in \{A_{\pm}, G, D\}$ are shown below. Despite the numerical hybridization of exciton states in the degenerate subspaces, the spin and orbital matrices in the exciton basis fully satisfy the symmetry considerations, clearly visible in the blocks with zero elements (between A and G/D for $\mathbf{B} \parallel z$ and within the A and G/D blocks for $\mathbf{B} \parallel x, y$).

Sigma-x =

```
[ 0.00+0.00j 0.00+0.00j 0.07+0.14j 0.03+0.07j]
[ 0.00+0.00j 0.00+0.00j -0.12+0.12j -0.03+0.04j]
[ 0.07-0.14j -0.12-0.12j 0.00+0.00j 0.00+0.00j]
[ 0.03-0.07j -0.03-0.04j 0.00+0.00j 0.00+0.00j]
```

Sigma-y =

```
[ 0.00+0.00j 0.00+0.00j -0.15+0.07j -0.04+0.03j]
[-0.00+0.00j 0.00+0.00j -0.11-0.10j -0.05-0.06j]
[-0.15-0.07j -0.11+0.10j 0.00+0.00j 0.00+0.00j]
[-0.04-0.03j -0.05+0.06j 0.00+0.00j -0.00+0.00j]
```

Sigma-z =

```
[-0.04+0.00j -0.62+1.81j 0.00+0.00j -0.00+0.00j]
[-0.62-1.81j 0.04+0.00j -0.00+0.00j 0.00+0.00j]
[-0.00+0.00j 0.00+0.00j -0.02+0.00j -0.02-0.00j]
[ 0.00+0.00j -0.00+0.00j -0.02+0.00j 0.02+0.00j]
```

L-x =

```
[ 0.00+0.00j 0.00+0.00j -0.01-0.03j -0.01-0.02j]
[ 0.00+0.00j 0.00+0.00j 0.03-0.02j 0.01-0.01j]
[-0.01+0.03j 0.03+0.02j 0.00+0.00j 0.00+0.00j]
[-0.01+0.02j 0.01+0.01j 0.00+0.00j 0.00+0.00j]
```

L-y =

```
[ 0.00+0.00j 0.00+0.00j 0.03-0.02j 0.01-0.01j]
[-0.00-0.00j 0.00+0.00j 0.02+0.02j 0.01+0.01j]
[ 0.03+0.02j 0.02-0.02j 0.00+0.00j -0.00+0.00j]
[ 0.01+0.01j 0.01-0.01j 0.00+0.00j 0.00+0.00j]
```

L-z =

```
[-0.04+0.00j -0.65+1.90j 0.00+0.00j 0.00+0.00j]
[-0.65-1.90j 0.05+0.00j 0.00+0.00j -0.00+0.00j]
[ 0.00+0.00j -0.00+0.00j -1.24+0.00j -1.20-0.01j]
[ 0.00+0.00j 0.00+0.00j -1.20+0.01j 1.24+0.00j]
```

V. ADDITIONAL FIGURES

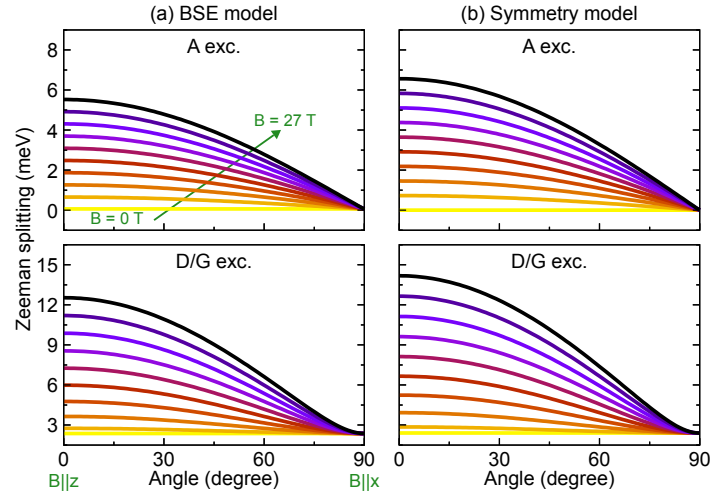


Fig. S1. Zeeman splitting of the A and D/G excitons as a function of the angle for different values of magnetic field for (a) the BSE model and (b) the symmetry-adapted model.

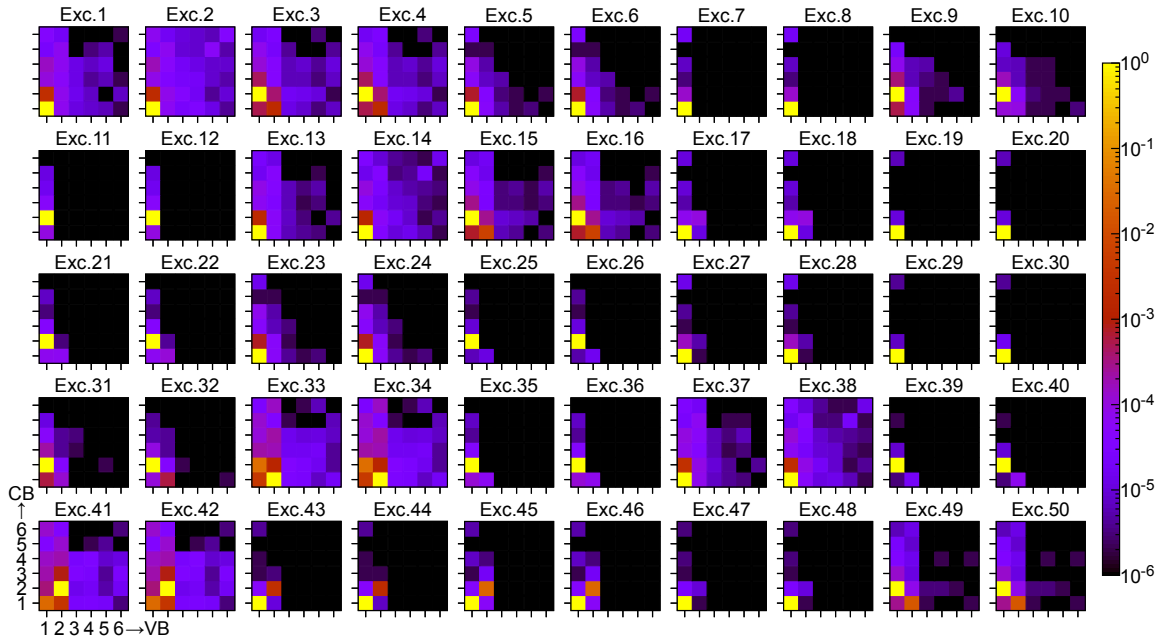


Fig. S2. Band composition of the exciton wavefunctions.

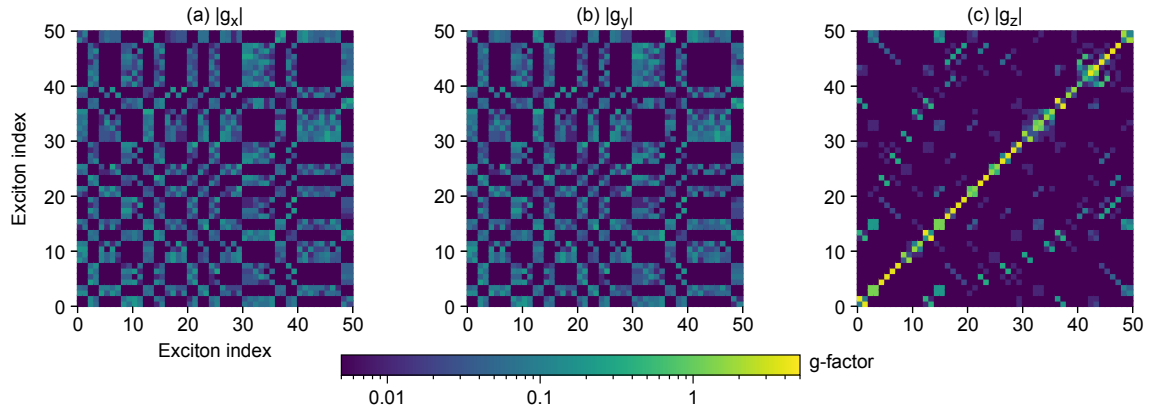


Fig. S3. Exciton g-factor matrix

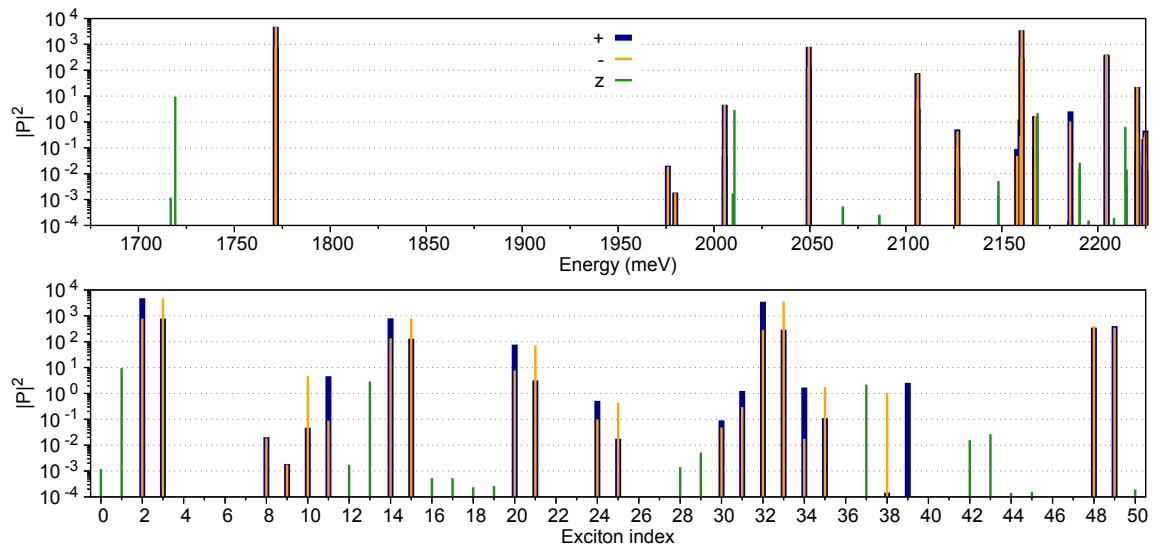


Fig. S4. Oscillator strength for various excitonic states.

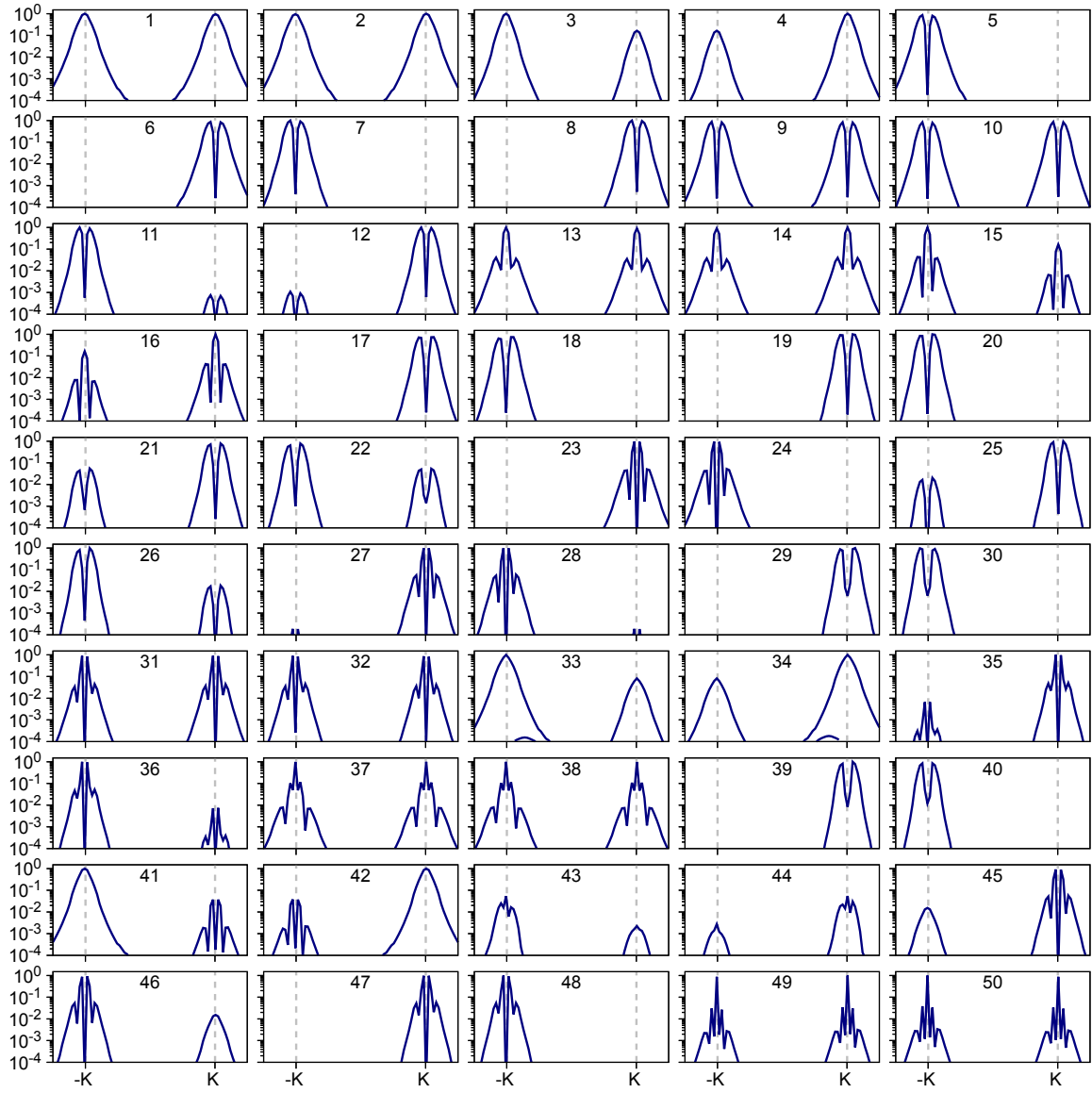


Fig. S5. Density of the exciton wavefunctions.

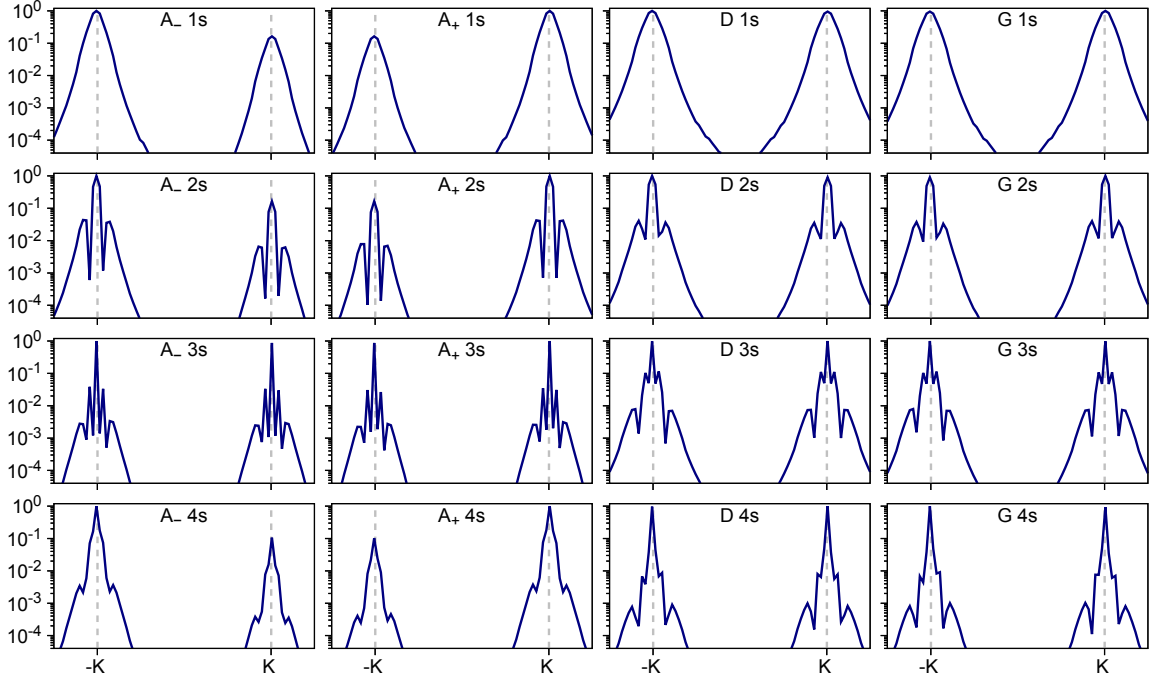


Fig. S6. Density of the A, D, and G 1s–4s exciton wavefunctions.

-
- [1] W. Schutte, J. De Boer, and F. Jellinek, Crystal structures of tungsten disulfide and diselenide, *J. Solid State Chem.* **70**, 207 (1987).
- [2] M. Camarasa-Gómez, A. Ramasubramaniam, J. B. Neaton, and L. Kronik, Transferable screened range-separated hybrid functionals for electronic and optical properties of van der Waals materials, *Phys. Rev. Mater.* **7**, 104001 (2023).
- [3] P. Giannozzi, S. Baroni, N. Bonini, M. Calandra, R. Car, C. Cavazzoni, D. Ceresoli, G. L. Chiarotti, M. Cococcioni, I. Dabo, A. Dal Corso, S. de Gironcoli, S. Fabris, G. Fratesi, R. Gebauer, U. Gerstmann, C. Gougoussis, A. Kokalj, M. Lazzeri, L. Martin-Samos, N. Marzari, F. Maurim, R. Mazzarello, S. Paolini, A. Pasquarello, L. Paulatto, C. Sbraccia, S. Scandolo, G. Sclauzero, A. P. Seitsonen, A. Smogunov, P. Umari, and R. M. Wentzcovitch, QUANTUM ESPRESSO: a modular and open-source software project for quantum simulations of materials, *J. Phys. Condens. Matter* **21**, 395502 (2009).
- [4] P. Giannozzi, O. Andreussi, T. Brumme, O. Bunau, M. Buongiorno Nardelli, M. Calandra,

- R. Car, C. Cavazzoni, D. Ceresoli, M. Cococcioni, N. Colonna, I. Carnimeo, A. Dal Corso, S. de Gironcoli, P. Delugas, R. A. DiStasio, A. Ferretti, A. Floris, G. Fratesi, G. Fugallo, R. Gebauer, U. Gerstmann, F. Giustino, T. Gorni, J. Jia, M. Kawamura, H.-Y. Ko, A. Kokalj, E. Küçükbenli, M. Lazzeri, M. Marsili, N. Marzari, F. Mauri, N. L. Nguyen, H.-V. Nguyen, A. Otero-de-la Roza, L. Paulatto, S. Poncé, D. Rocca, R. Sabatini, B. Santra, M. Schlipf, A. P. Seitsonen, A. Smogunov, I. Timrov, T. Thonhauser, P. Umari, N. Vast, X. Wu, and S. Baroni, Advanced capabilities for materials modelling with Quantum ESPRESSO, *J. Phys. Condens. Matter* **29**, 465901 (2017).
- [5] P. Giannozzi, O. Baseggio, P. Bonfà, D. Brunato, R. Car, I. Carnimeo, C. Cavazzoni, S. de Gironcoli, P. Delugas, F. Ferrari Ruffino, A. Ferretti, N. Marzari, I. Timrov, A. Urru, and S. Baroni, Quantum ESPRESSO toward the exascale, *J. Chem. Phys.* **152**, 154105 (2020).
- [6] J. P. Perdew, K. Burke, and M. Ernzerhof, Generalized gradient approximation made simple, *Phys. Rev. Lett.* **77**, 3865 (1996).
- [7] M. J. van Setten, M. Giantomassi, E. Bousquet, M. J. Verstraete, D. R. Hamann, X. Gonze, and G.-M. Rignanese, The pseudodojo: Training and grading a 85 element optimized norm-conserving pseudopotential table, *Comput. Phys. Commun.* **226**, 39 (2018).
- [8] P. Blaha, K. Schwarz, F. Tran, R. Laskowski, G. K. Madsen, and L. D. Marks, Wien2k: An APW+lo program for calculating the properties of solids, *J. Chem. Phys.* **152**, 074101 (2020).
- [9] K. Lejaeghere, G. Bihlmayer, T. Björkman, P. Blaha, S. Blügel, V. Blum, D. Caliste, I. E. Castelli, S. J. Clark, A. D. Corso, S. de Gironcoli, T. Deutsch, J. K. Dewhurst, I. D. Marco, C. Draxl, M. Duřak, O. Eriksson, J. A. Flores-Livas, K. F. Garrity, L. Genovese, P. Giannozzi, M. Giantomassi, S. Goedecker, X. Gonze, O. Grånäs, E. K. U. Gross, A. Gulans, F. Gygi, D. R. Hamann, P. J. Hasnip, N. A. W. Holzwarth, D. Iuşan, D. B. Jochym, F. Jollet, D. Jones, G. Kresse, K. Koepnik, E. Küçükbenli, Y. O. Kvashnin, I. L. M. Locht, S. Lubeck, M. Marsman, N. Marzari, U. Nitzsche, L. Nordström, T. Ozaki, L. Paulatto, C. J. Pickard, W. Poelmans, M. I. J. Probert, K. Refson, M. Richter, G.-M. Rignanese, S. Saha, M. Scheffler, M. Schlipf, K. Schwarz, S. Sharma, F. Tavazza, P. Thunström, A. Tkatchenko, M. Torrent, D. Vanderbilt, M. J. van Setten, V. V. Speybroeck, J. M. Wills, J. R. Yates, G.-X. Zhang, and S. Cottenier, Reproducibility in density functional theory calculations of solids, *Science* **351**, aad3000 (2016).
- [10] D. J. Singh and L. Nordstrom, *Planewaves, Pseudopotentials, and the LAPW method*

- (Springer Science & Business Media, 2006).
- [11] J. Deslippe, G. Samsonidze, D. A. Strubbe, M. Jain, M. L. Cohen, and S. G. Louie, BerkeleyGW: A massively parallel computer package for the calculation of the quasiparticle and optical properties of materials and nanostructures, *Comput. Phys. Commun.* **183**, 1269 (2012).
 - [12] M. Rohlfing and S. G. Louie, Electron-hole excitations in semiconductors and insulators, *Phys. Rev. Lett.* **81**, 2312 (1998).
 - [13] M. Rohlfing and S. G. Louie, Electron-hole excitations and optical spectra from first principles, *Phys. Rev. B* **62**, 4927 (2000).
 - [14] M. Wu, *Spin-Orbit Coupling, Broken Time-Reversal Symmetry, and Polarizability Self-Consistency in GW and GW-BSE Theory with Applications to Two-Dimensional Materials*, Ph.D. thesis, University of California, Berkeley (2020).
 - [15] M. S. Hybertsen and S. G. Louie, Electron correlation in semiconductors and insulators: Band gaps and quasiparticle energies, *Phys. Rev. B* **34**, 5390 (1986).
 - [16] B. A. Barker, J. Deslippe, J. Lischner, M. Jain, O. V. Yazyev, D. A. Strubbe, and S. G. Louie, Spinor GW/Bethe-Salpeter calculations in BerkeleyGW: Implementation, symmetries, benchmarking, and performance, *Phys. Rev. B* **106**, 115127 (2022).
 - [17] F. H. da Jornada, D. Y. Qiu, and S. G. Louie, Nonuniform sampling schemes of the Brillouin zone for many-electron perturbation-theory calculations in reduced dimensionality, *Phys. Rev. B* **95**, 035109 (2017).
 - [18] S. Ismail-Beigi, Truncation of periodic image interactions for confined systems, *Phys. Rev. B* **73**, 233103 (2006).
 - [19] T. Woźniak, P. E. Faria Junior, G. Seifert, A. Chaves, and J. Kunstmann, Exciton g -factors of van der Waals heterostructures from first-principles calculations, *Phys. Rev. B* **101**, 235408 (2020).
 - [20] T. Amit, D. Hernangómez-Pérez, G. Cohen, D. Y. Qiu, and S. Refaely-Abramson, Tunable magneto-optical properties in MoS₂ via defect-induced exciton transitions, *Phys. Rev. B* **106**, L161407 (2022).
 - [21] P. E. Faria Junior, K. Zollner, T. Woźniak, M. Kurpas, M. Gmitra, and J. Fabian, First-principles insights into the spin-valley physics of strained transition metal dichalcogenides monolayers, *New J. Phys.* **24**, 083004 (2022).
 - [22] P. E. Faria Junior, T. Naimer, K. M. McCreary, B. T. Jonker, J. J. Finley, S. A. Crooker,

- J. Fabian, and A. V. Stier, Proximity-enhanced valley Zeeman splitting at the WS₂/graphene interface, *2D Mater.* **10**, 034002 (2023).
- [23] L. Kipczak, A. O. Slobodeniuk, T. Woźniak, M. Bhatnagar, N. Zawadzka, K. O. Pucko, M. J. Grzeszczyk, K. Watanabe, T. Taniguchi, A. Babinski, and M. Molas, Analogy and dissimilarity of excitons in monolayer and bilayer of MoSe₂, *2D Mater.* , 025014 (2023).
- [24] N. S. Rytova, Screened potential of a point charge in a thin film, *Moscow University Physics Bulletin* **3**, 30 (1967).
- [25] L. V. Keldysh, Coulomb interaction in thin semiconductor and semimetal films, *JETP Lett.* **29**, 658 (1979).
- [26] A. Laturia, M. L. Van de Put, and W. G. Vandenberghe, Dielectric properties of hexagonal boron nitride and transition metal dichalcogenides: from monolayer to bulk, *npj 2D Mater. Appl.* **2**, 6 (2018).
- [27] T. Deilmann, P. Krüger, and M. Rohlfing, Ab initio studies of exciton g factors: Monolayer transition metal dichalcogenides in magnetic fields, *Phys. Rev. Lett.* **124**, 226402 (2020).
- [28] Y. G. Gobato, C. S. de Brito, A. Chaves, M. A. Prosnikov, T. Woźniak, S. Guo, I. D. Barcelos, M. V. Milošević, F. Withers, and P. C. M. Christianen, Distinctive g -factor of moiré-confined excitons in van der Waals heterostructures, *Nano Lett.* **22**, 8641 (2022).
- [29] J. Ruan, Z. Li, C. S. Ong, and S. G. Louie, Optically controlled single-valley exciton doublet states with tunable internal spin structures and spin magnetization generation, *PNAS* **120**, e2307611120 (2023).
- [30] J. J. Esteve-Paredes, M. A. García-Blázquez, A. J. Uría-Álvarez, M. Camarasa-Gómez, and J. J. Palacios, Excitons in nonlinear optical responses: shift current in MoS₂ and GeS monolayers, *npj Comput. Mater.* **11**, 13 (2025).
- [31] Y. Yafet, g factors and spin-lattice relaxation of conduction electrons, in *Solid state physics*, Vol. 14 (Elsevier, 1963).
- [32] S. Bhowal and G. Vignale, Orbital hall effect as an alternative to valley hall effect in gapped graphene, *Phys. Rev. B* **103**, 195309 (2021).
- [33] A. Urru, O. P. O. Ivo Souza, S. S. Tsirkin, and D. Vanderbilt, Optical spatial dispersion via wannier interpolation, [arXiv:2504.09742](https://arxiv.org/abs/2504.09742) (2025).
- [34] G. F. Koster, J. O. Dimmock, R. G. Wheeler, and H. Statz, *Properties of the thirty-two point groups*, Vol. 24 (MIT press, 1963).

- [35] M. Kurpas, M. Gmitra, and J. Fabian, Spin-orbit coupling and spin relaxation in phosphorene: Intrinsic versus extrinsic effects, *Phys. Rev. B* **94**, 155423 (2016).
- [36] M. Kurpas, P. E. Faria Junior, M. Gmitra, and J. Fabian, Spin-orbit coupling in elemental two-dimensional materials, *Phys. Rev. B* **100**, 125422 (2019).
- [37] J. V. V. Cassiano, A. de Lelis Araújo, P. E. Faria Junior, and G. J. Ferreira, Dft2kp: Effective kp models from ab-initio data, *SciPost Physics Codebases* **25**, 10.21468/scipostphyscodeb.25 (2024).
- [38] S. Zhang, H. Sheng, Z.-D. Song, C. Liang, Y. Jiang, S. Sun, Q. Wu, H. Weng, Z. Fang, X. Dai, *et al.*, Vasp2kp: k-p models and Landé g-factors from ab initio calculations, *Chin. Phys. Lett.* **40**, 127101 (2023).
- [39] C. Robert, T. Amand, F. Cadiz, D. Lagarde, E. Courtade, M. Manca, T. Taniguchi, K. Watanabe, B. Urbaszek, and X. Marie, Fine structure and lifetime of dark excitons in transition metal dichalcogenide monolayers, *Phys. Rev. B* **96**, 155423 (2017).
- [40] M. R. Molas, C. Faugeras, A. O. Slobodeniuk, K. Nogajewski, M. Bartos, D. M. Basko, and M. Potemski, Brightening of dark excitons in monolayers of semiconducting transition metal dichalcogenides, *2D Mater.* **4**, 021003 (2017).
- [41] M. R. Molas, A. O. Slobodeniuk, T. Kazimierzuk, K. Nogajewski, M. Bartos, P. Kapuściński, K. Oreszczuk, K. Watanabe, T. Taniguchi, C. Faugeras, P. Kossacki, D. M. Basko, and M. Potemski, Probing and manipulating valley coherence of dark excitons in monolayer WSe₂, *Phys. Rev. Lett.* **123**, 096803 (2019).